JOURNAL OF SOLID STATE CHEMISTRY 119, 260–270 (1995)

On the Cubic Perovskites $La_{0.2}Sr_{0.8}Cu_{0.4}M_{0.6}O_{3-y}$ (M = Co, Fe)

R. Genouel, C. Michel, N. Nguyen, F. Studer, M. Hervieu, and B. Raveau

Laboratoire CRISMAT, CNRS URA 1318-ISMRA, Université de Caen, Boulevard du Maréchal Juin, 14050 Caen Cedex, France

Received January 3, 1995; in revised form May 5, 1995; accepted May 8, 1995

A new oxygen-deficient perovskite $La_{0.2}Sr_{0.8}Cu_{0.4}M_{0.6}O_{3-y}$ (M = Co, Fe) has been synthesized that exhibits a large concentration of oxygen vacancies ($0.3 \leq y \leq 0.58$). Despite this, X-ray powder diffraction shows no superstructure of the primitive cell, indicating a random distribution of the vacancies on the oxygen sites. This result has been confirmed by electron diffraction and high-resolution microscopy, which show that most of the crystals exhibit the regular perovskite cell. In the cobalt phase, X-ray absorption spectroscopy at CoK-, CuK- and CuL_3-edges has shown that cobalt is in the Co(III) valence state even after oxygen annealings and that copper is in a mixed valence state, Cu(II)/Cu(III). In contrast, in the iron phase, which is less oxygen deficient than the cobalt phase, Mössbauer spectroscopy has shown that iron exhibits a mixed valence state, Fe(III)/Fe(IV). The conductivity of this new phase exhibits a transition from a semiconducting to a semimetallic behavior; it increases after oxygen annealings, in agreement with the increase in the hole density, i.e., the Cu(III) content. © 1995 Academic Press, Inc.

INTRODUCTION

A great deal of work was devoted to the oxygen-deficient perovskites ABO_{3-x} with B = Fe, Co, Cu, much of it done before the discovery of superconductivity in copper oxides. The interest in these compounds rests in their electron transport and magnetic properties, which are closely related to the mixed valence of the transition element: Fe(III)/Fe(IV), Co(III)/Co(IV), and Cu(II)/Cu(III). In fact, the mixed valence of the transition element in these phases is itself related to the ability of the transition element to adopt various coordinations—octahedral, tetrahedral, pyramidal, and square plane—so that the deviation from the perfect stoichiometry "O_3" may vary dramatically. This is for instance the case in iron oxides $SrFeO_{3-x}$ (1, 2), many lanthanum barium and lanthanum strontium cuprates (3–9), and cobalt oxides $SrCoO_{3-x}$ (10). One striking feature of these perovskites is that most of them are characterized by an ordering of the oxygen and anionic vacancies so that tunnel structures or layered structures are generated.

Only a few oxygen-deficient perovskites of these elements exhibit a single cubic cell, which would imply a disordering of the oxygen vacancies. Such a phenomenon has recently been observed by "mixing" iron and copper on the B sites. In this way, two series of oxygen deficient perovskites, $AFe_{1-x}Cu_xO_{2.5-x/2+\delta}$ (A = Ba, Sr) (11) and $Ba_{0.5}La_{0.5}Fe_{1-x}Cu_xO_{2.75-x/2+\delta}$ (12), with a cubic symmetry have indeed been synthesized, in spite of the large rate of oxygen vacancies (close to 0.6 per unit cell). Nevertheless, the electron diffraction observations show that, in addition to these cubic crystals, there exist many crystals that exhibit superstructures. In contrast, the substitution of iron for copper in the oxygen-deficient perovskite $Sr_{1.6+x}La_{6.4-x}Cu_{8-x}Fe_xO_{20}$ ($0 \leq x \leq 2$) keeps the oxygen and vacancies ordering of this tetragonal phase (13), whose lattice parameters are connected to that of the cubic perovskite a_p by the relations $a = b = 2a_p\sqrt{2}$, $c = a_p$. However, for higher iron contents, a new cubic perovskite is evidenced by a variation of the oxygen content. This paper deals with the study of this new phase, and of the homologous cobalt compound, formulated $La_{0.2}Sr_{0.8}Cu_{0.4}M_{0.6}O_{3-y}$, with M = Co, Fe.

SYNTHESIS AND EXPERIMENTAL

The syntheses were realized by solid state reaction from predried oxides La_2O_3, CuO, Fe_2O_3, $Co_3O_{4.2}$, and strontium carbonate $SrCO_3$, mixed in stoichiometric ratios. Mixtures were heated in a platinum crucible in air at 1000°C for 24 hr and then quenched to room temperature.

X-ray data were collected by step scanning in the range $20° \leq 2\theta \leq 100°$ with an increment of 0.02° (2θ). Lattice constants were determined by the Rietveld method (computer program D.B.W. 3.2 (14) from X-ray powder diffraction patterns obtained with a Philips diffractometer with Cu$K\alpha$ radiation.

The electron diffraction study was carried out with a JEOL 200CX electron microscope fitted with a eucentric goniometer (±60°); high-resolution electron microscopy was performed with a TOPCON 0002B, with a resolution point of 1.8 Å.

The oxygen content of the iron-substituted phases was determined by chemical analysis using a redox back titration method. Tetravalent iron and trivalent copper, if pres-

0022-4596/95 $12.00

ent, were reduced to Fe(III) and Cu(II) by a known amount of iron (II) chloride in acid solution. Unreacted Fe(II) was determined by back titration with potassium dichromate. The oxygen content of the cobalt-substituted phases was determined by thermogravimetric analysis. Samples were reduced in a 90% Ar + 10% H_2 gas flow at 980°C for 8 hr using a Setaram TAG 24 microbalance for weight loss measurements.

The magnetic susceptibility was measured by the Faraday method in the temperature range 77 K $\leq T \leq$ 700 K, using a Setaram MTB 10-8 balance. The Mössbauer resonance spectrum of the iron-substituted compound was recorded at room temperature, using a constant acceleration spectrometer with a ^{57}Co/Rh source in a transmission geometry. The isomer shifts are given with respect to metallic iron at room temperature.

The resistivity measurements were performed in the temperature range 80–280 K, using a classical four-probe method on samples sintered in the form of bars (12 × 2 × 1 mm^3) at 1000°C in air and then quenched to room temperature. Postannealing treatments were performed at 450°C on the as-prepared samples under different oxygen pressures (1, 10 and 100 bars, respectively) for 24 hr in order to achieve thermodynamic equilibrium. Samples were introduced in a cryostat and data were collected every 2 K. The cooling rate was fixed to 60 K/hr.

The XAS spectra at the Co*K*-edge were recorded at room temperature on powder samples in transmission mode. The experiments were performed at LURE (Orsay), using the synchrotron radiation from the DCI storage ring operated at 1.85 GeV with a nominal current of 250 mA. X-rays were monochromatized by a Si (331) channel cut and the incident and transmitted intensities were measured by using two ionization chambers. The energy resolution was estimated to be better than 0.8 eV at the Co*K*-edge whereas the reproducibility of the energy position of the spectral features was close to 0.3 eV.

The normalization procedure used throughout this work was a standard one: after subtraction of the same background from the XANES and EXAFS spectra, recorded under the same experimental conditions, a point located at an energy of 800 eV from the edge, where no more EXAFS oscillations were observable, was set to unity.

XAS spectra at the L_3-edge of copper were recorded at room temperature on powder samples by a fluorescence yield method. The experiments were performed at LURE (Orsay), using the synchrotron radiation from the super-ACO ring operated at 800 MeV with a typical current of 250 mA. Samples were ground and sieved homogeneously on a sticky band supported by an aluminum sample holder. Electrical contacts were realized by silver paste dots. The X-rays were monochromatized by two beryl crystals ($10\bar{1}0$), focused by a TiN-coated parabolic mirror to generate a 0.5-mm diameter spot, and the total electron yield was detected by a measure of the induced current through the sample. The energy scale was then fixed with respect to the $|3d^9\rangle$ peak of CuO at 931.2 eV. The experimental energy resolution was estimated to be better than 0.3 eV, whereas the reproducibility of the energy position of the spectral features is close to 0.05 eV. The width of the core hole has been measured to be 0.3 eV at the L_3-edge. The usual thickness of the probed upper layer of the samples is about 200 Å in the total electron yield mode. The top of the $|3d^9\rangle$ transitions for all the compounds has been set to a common value chosen arbitrarily.

TABLE 1
Analytical Results (Oxygen Nonstoichiometry and Lattice Parameters) for $La_{0.2}Sr_{0.8}Cu_{0.4}M_{0.6}O_{3-y}$ (M = Fe, Co)

	M = Fe		M = Co	
	$y \pm 0.01$	$a \pm 0.0004$ (Å)	$y \pm 0.01$	$a \pm 0.0004$ (Å)
a.s.[a]	0.36	3.8589	0.58	3.8579
O[2]	0.33	3.8574	0.49	3.8504
10b	0.30	3.8557	0.38	3.8469
100b	0.30	3.8558	0.34	3.8457

[a] a.s. denotes the as-synthesized sample.

RESULTS AND DISCUSSION

1. Structural Characterization

For both series $La_{0.8-x}Sr_{0.2+x}Cu_{1-x}M_xO_{3-y}$, M = Co, Fe, single-phase samples are obtained for x ranging from 0.53 to 0.63. The X-ray diffraction patterns are characteristic of a cubic perovskite cell with "a" close to 3.85 Å. For further investigations the composition $La_{0.2}Sr_{0.8}Cu_{0.4}M_{0.6}O_{3-y}$ has been chosen. The determination of the oxygen content reveals a large oxygen deficiency, especially for the cobalt-substituted material (Table 1). The absence of a superstructure in the X-ray diffraction pattern (Fig. 1), in spite of a high oxygen deficiency, is confirmed by electron microscopy. The reconstruction of the reciprocal space has been performed on numerous grains of both iron- and cobalt-substituted samples. It shows that the samples are well crystallized and that most of the crystals exhibit a cubic cell, with $a \approx a_p$ and no condition limiting the reflection. This is illustrated in Fig. 2a where a [001] electron diffraction (ED) pattern is presented. The corresponding [001] HREM image (Fig. 3) exhibits a contrast which is classically observed in the perovskite-type oxides; it consists in a very regular array of bright dots, spaced by 2.75 Å along ⟨110⟩. Such images attest to a statistical distribution of the cations on the one hand, and of the oxygens and vacancies on the other hand, over their respective sites.

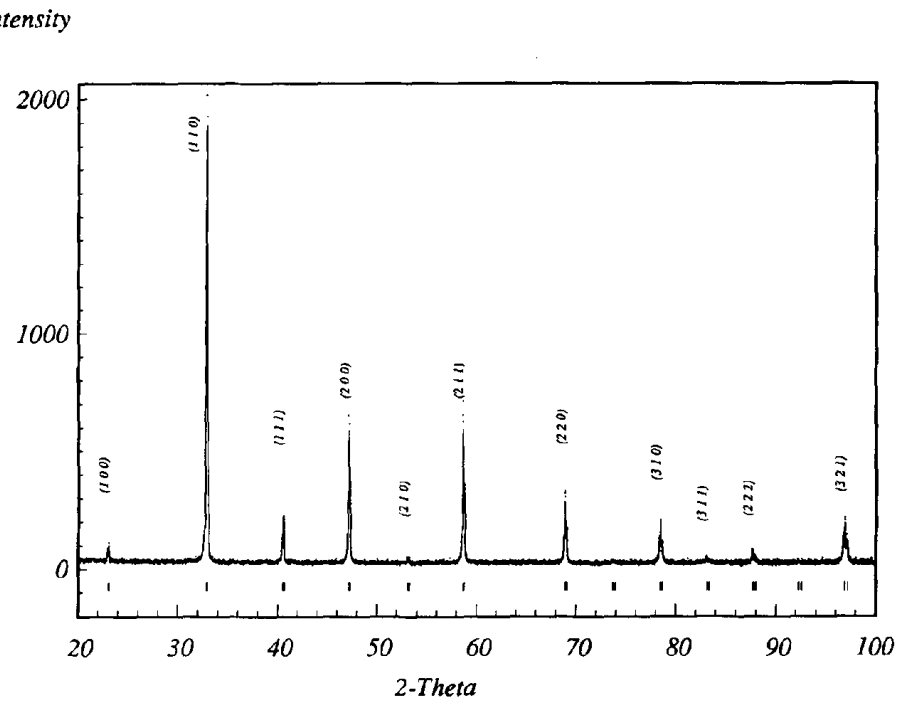

FIG. 1. X-ray powder diffraction pattern of $La_{0.2}Sr_{0.8}Cu_{0.4}Co_{0.6}O_{3-y}$, as-synthesized sample, with indices for some diffraction peaks. Small bars indicate the Bragg angle positions.

However, some crystals exhibit [001] ED patterns where weak and diffuse satellites are associated with the basic perovskite spots. They are observed along the $\langle 110\rangle^*$ and $\langle 1\bar{1}0\rangle^*$ directions. The first-order satellites are in positions close to 1/4, 1/4, 0; −1/4, 3/4, 0; −3/4, 1/4, 0; and 3/4, 3/4, 0. An example is shown in Fig. 2b for the iron-substituted sample but a similar feature is observed in the cobalt sample; the satellites around the (210) reflection are marked by arrowheads. The high-resolution images recorded along that direction show the presence of modulations (Fig. 4). The square mesh of bright dots is the basic lattice (2.5 × 2.5 Å^2) but we can observe that the dots vary in brightness along the $\langle 110\rangle$ and $\langle 1\bar{1}0\rangle$ directions. These variations in the contrast are always locally established in very small areas of the matrix. The most frequently observed pseudoperiodicity is $4 \times d_{110}$ (as an example, see arrowheads in Fig. 4) but, in most of the crystals, no real superstructure is revealed, due to the high degree of perturbation in the ordering. These observations are consistent with the existence of the very weak and diffuse satellites in the ED patterns. These modulations are correlated to short-range order–disorder phenomena.

Considering that La and Sr on the one hand and Fe, Co, and Cu on the other hand exhibit, respectively, very close scattering factors, such variations in the contrast would result from the local arrangement of oxygen and vacancies, and from the induced cationic displacements. The EDS analysis performed on such crystals does not allow significant variations in the cation ratios to be evidenced; moreover, various annealings (in air, under oxygen flow) coupled with slow cooling do not allow a new superstructure to be stabilized for the corresponding nominal composition; this suggests that the local short-range orderings which have been observed are correlated to very metastable microphases.

Annealing under argon at low temperature (450°C) leads to a progressive decomposition of the phase associated with an oxygen loss. For example, electron diffraction analysis of a 12-hr argon-annealed sample of $La_{0.2}Sr_{0.8}Cu_{0.4}Fe_{0.6}O_{3-y}$ evidences the formation of a complex multiphased material containing, in addition to the original cubic oxide, tetragonal phases of the systems $La_{2-x}Sr_xCuO_4$, $Sr_{1.6+x}La_{6.4-x}Cu_{8-x}Fe_xO_{20}$, and a perovskite $SrFe_{1-x}Cu_xO_y$ (11).

In order to test the influence of oxygen stoichiometry upon lattice constants and then on electrical properties, annealing treatments under different oxygen pressures have been performed at 450°C for 24 hr: oxygen flow (denoted O_2), and 10 bars and 100 bars oxygen pressure (denoted 10b and 100b, respectively). The resulting oxygen stoichiometries and lattice constants are listed in Table 1. Whatever the annealing conditions, the oxygen content and cell parameters do not vary dramatically in the case of iron substitution. In contrast, the cobalt-substituted material is sensitive to oxygen pressure during the annealings, as can be seen from the oxygen stoichiometry

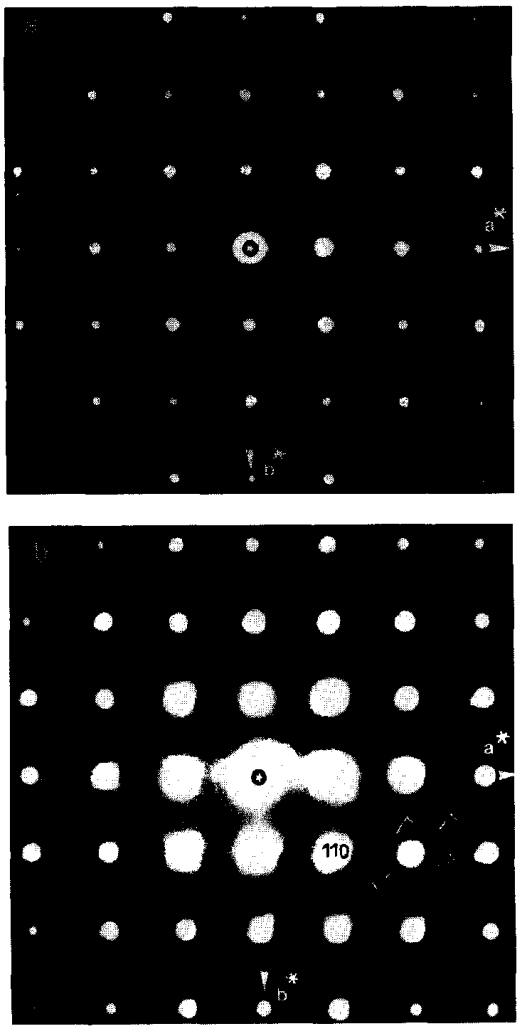

FIG. 2. (a) Typical [001] ED pattern recorded for $La_{0.2}Sr_{0.8}Cu_{0.4}Fe_{0.6}O_{3-y}$. (b) Weak and diffuse satellites (arrowheads), lying along ⟨110⟩*.

and lattice constant measurements. Note that in both systems the lattice parameter a decreases when the oxygen content increases, in agreement with the increase in the oxidation state of the B cation.

2. X-Ray Absorption Spectroscopy

XANES spectroscopy has been proved to be a valuable tool in the determination of the electronic structure above the Fermi level (first empty levels) and of the valence state of the elements in solids (15–22). In order to obtain further information about the valence states of the metallic cations in the $La_{0.2}Sr_{0.8}Cu_{0.4}Co_{0.6}O_{3-y}$ oxide as synthesized and after heating treatments, we have performed XAS measurements at CoK-, CuK-, and CuL_3-edges. Considering the small variations in oxygen deficiencies under annealing treatments of the $La_{0.2}Sr_{0.8}Cu_{0.4}Fe_{0.6}O_{3-y}$ oxide, the iron K-edge has not been taken into account for this study.

2a. The Cobalt Valence

In oxides, cobalt can be found mainly in the Co(II) and Co(III) valence states. Co(II) appears most of the time as a high spin $3d^7$ cation. As for copper, the real electronic configuration of Co(II) can be written $\alpha\,|3d^7\rangle + \beta\,|3d^8\underline{L}\rangle$ taking into account the Co–O covalence through the charge-transfer model but here $\beta < \alpha$ (23). The increase in the cobalt charge induces a decrease in the Co–O distance which increases the covalency of the Co–O bond and thus the real ground state electronic configuration for Co(III) can be written $\alpha\,|3d^6\rangle + \beta\,|3d^7\underline{L}\rangle$ with a strong contribution of the latter. A more detailed analysis of the CoK-edges for many Co(II) and Co(III) oxides has been presented previously (24, 25). In the present work, we have chosen cobalt carbonate $CoCO_3$, isotypic to calcite, as a reference for Co(II) in a slightly distorted octahedron ($d_{Co-O} \approx 2.02$ Å) and $LaCoO_3$ for Co(III) in a regular octahedron ($d_{Co-O} \approx 1.92$ Å) (26).

Reference compounds. At the CoK-edge, $CoCO_3$ exhibits a very simple spectrum (Fig. 5) with a main white line at 15.5 eV corresponding to the $|1s^2 3d^7 4p^0\rangle \rightarrow |1s^1 3d^7 4p^1\rangle$ electronic transition. A very weak prepeak A can be observed around 1 eV, probably due to some quadrupolar effect since the $1s \rightarrow 3d$ transition is dipole forbidden.

The compound $LaCoO_3$ has been synthesized at normal oxygen pressure at 900°C. By thermogravimetric analysis, the oxygen stoichiometry has been shown to be $LaCoO_{3\pm0.03}$ and the cobalt valence is thus close to III. The $LaCoO_3$ spectrum (Fig. 5) exhibits only a white line at 18 eV, corresponding to the $|1s^2 3d^6 4p^0\rangle \rightarrow |1s^1 3d^6 4p^1\rangle$ electronic transition. The prepeak A is more intense than in $CoCO_3$, which suggests that a slight distortion of the CoO_6 octahedra occurs; it exhibits a two-peak structure which can be correlated to the Co $3d(t_{2g})$ and $3d(e_g)$ orbitals and shows that Co(III) cannot be in the low-spin state in this compound.

A large energy shift is observed between the $CoCO_3$ and the $LaCoO_3$ spectra, in agreement with their respective cobalt valences. A quantitative analysis of the edge positions can be realized using a method proposed first by Alp *et al.* (16) in which the real spectrum is replaced by an equivalent square-shaped edge whose energy position can be estimated. Such an analysis has been performed on both reference edges presented here and the results (Table 2) show that a large energy shift exists between the Co(II) and the Co(III) references ($\Delta E \approx 3.6$ eV). In a previous paper (25), we have shown that the edge energies of all the references for Co(II), namely $CoCO_3$, $CoAl_2O_4$, and La_2CoO_4 are close together around 7 eV.

FIG. 3. Typical [001] HREM image recorded for $La_{0.2}Sr_{0.8}Cu_{0.4}Fe_{0.6}O_{3-y}$. A very regular contrast is observed, which attests to the statistical distribution of the cations and of the anions and vacancies over their respective sites.

The $La_{0.2}Sr_{0.8}Cu_{0.4}Co_{0.6}O_{3-y}$ *oxide.* XANES have been performed at the Co*K*-edge on two samples: the as-synthesized sample and the sample annealed at 450°C for 24 h under 1 bar oxygen pressure. The spectra are also presented in Fig. 5 with the reference compounds and the equivalent energies in Table 2. Both are very similar; their equivalent energies are close to that of $LaCoO_3$, suggesting a Co(III) valence state, but they show a significant increase in the prepeak A intensity and a strong decrease in the main line intensity with respect to La CoO_3. The increase in the prepeak intensity in 3*d* transition metal compounds has been shown to be linked to the existence of noncentrosymmetric polyhedra around the photoexcited metal and the main line intensity, which mainly reflects the empty Co–O antibonding orbitals, depends strongly on the number of oxygen first-neighbors. The latter characteristics suggest a less symmetric environment of cobalt in the $La_{0.2}Sr_{0.8}Cu_{0.4}Co_{0.6}O_{3-y}$ oxide than the regular octahedron in $LaCoO_3$, in agreement with the oxygen deficiency (see Table 1). The equivalent

FIG. 4. Modulations of the contrast, associated with the diffuse satellites (Fig. 2b). The pseudo-periodicity is 4^*d_{110} (black arrowheads).

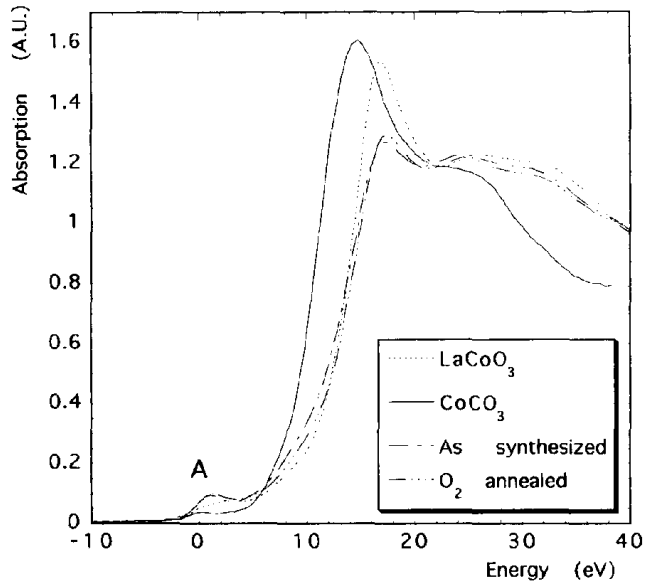

FIG. 5. The Co*K*-edges of CoCO3 and $LaCoO_3$, taken as references for Co(II) and Co(III) valence states, respectively, and of the $La_{0.2}Sr_{0.8}Cu_{0.4}Co_{0.6}O_{3-y}$ phase as synthesized and annealed at 450°C under 1 bar oxygen pressure for 24 hr.

energies of the cubic perovskite are close to that of La CoO_3, suggesting that cobalt exhibits the Co(III) valence state even after oxygen annealing.

2b. *The Copper Valence*

In oxides, as in HTC superconductors, copper can present simultaneously the three known valence states Cu(I), Cu(II), and Cu(III). The Cu *K*- and Cu L_3-edges of Cu_2O for Cu(I), and of La_2CuO_4 and Nd_2CuO_4 for Cu(II) have been recorded as references. The latter compounds exhibit a somewhat different copper coordination with an elongated oxygen octahedron for La_2CuO_4 and a square plane for Nd_2CuO_4, leading to a more pronounced z-polarized contribution in the copper *K*-edge spectrum for the latter. But, in both cases, the Cu $3d_{x^2-y^2}$ orbital is the only one which contains covalent holes. The detailed analysis of copper electronic configurations in various valence states has been published in many papers (27–34) and can be summarized in the following way: Cu(I) in the $3d^{10}$, Cu(II) in the $\alpha\,|3d^9\rangle + \beta\,|3d^{10}\underline{L}\rangle$ with $\beta > \alpha$, and Cu(III) in the $|3d^9\underline{L}\rangle$ configurations, respectively. The two latter configurations are due to a charge-transfer mechanism predominant in copper oxides.

The "Cu(I)" valence. At the Cu *K*-edge, the Cu_2O spectrum shows a peak at 1.3 eV (Fig. 6a) due to the $1s \rightarrow 4p$ transition in the $3d^{10}$ configuration and characteristic of Cu(I). Such a peak is totally absent either from the La_2CuO_4 spectrum or from the spectra of the $La_{0.2}Sr_{0.8}Cu_{0.4}Co_{0.6}O_{3-y}$ oxide as synthesized or annealed. Thus, one can conclude that there is an absence of Cu(I) in the $La_{0.2}Sr_{0.8}Cu_{0.4}Co_{0.6}O_{3-y}$ oxide with a precision better than 5%. A slight shift toward high energy of the spectrum of the O_2-annealed sample with respect to the as-synthesized sample reflects the oxidation of copper during annealing. Its value has been estimated through the calculation of an equivalent step energy based on the same method as that used above for cobalt (16, 33). Nevertheless, it is too small to precisely evaluate the mean copper charge.

The "Cu(II)" valence. The main peak in the Cu *K*-edge spectra is due to the strong antibonding orbital of the Cu–O bond in the $|3d^{10}\underline{L}\rangle$ configuration. Its intensity, directly related to the number of Cu–O bonds and the Cu–O distance is smaller in $La_{0.2}Sr_{0.8}Cu_{0.4}Co_{0.6}O_{3-y}$, as synthesized or annealed, than in La_2CuO_4. This result can be linked to a reduction in the number of oxygen first-neighbors in our phase compared to La_2CuO_4, in agreement with the oxygen deficiency.

The "Cu(III)" valence. At the Cu L_3-edge, the reference compound for Cu(II), Nd_2CuO_4, shows only one symmetric peak (Fig. 6b) due to the $|2p^63d^9\rangle \rightarrow |\underline{c}2p^53d^{10}\rangle$ transition. The CuL_3-edge spectrum of the compound La_2CuO_4 looks identical to that of Nd_2CuO_4. As has been shown by previous works (15, 18–21), the "Cu(III)" valence appears as a shoulder on the high-energy side of the main peak (≈933 eV), due to the $|2p^63d^9\underline{L}\rangle \rightarrow |c2p^53d^{10}\underline{L}\rangle$ transition. The Cu L_3-edge of the Cu(III) compound $La_2Li_{0.5}Cu_{0.5}O_4$ (34) has been shown to exhibit only the $|3d^9\underline{L}\rangle$ peak at 933.2 eV. Such a shoulder appears only as an asymmetry on the high energy side of the main peak

TABLE 2

Calculated Equivalent Energies for Co*K*- and Cu*K*-Edges and Doping Hole Densities n_h Estimated from the CuL_3-Edge for Some Reference Oxides and for the As-Synthesized (a.s.) and O_2 Annealed $La_{0.2}Sr_{0.8}Cu_{0.4}Co_{0.6}O_{3-y}$ Perovskite (P)

Compounds	*S* (eV) for Co*K*-edge	Compounds	*S* (eV) for Cu*K*-edge	Compounds	n_h for CuL_3-edge
$CoCO_3$	6.8	Cu_2O	2.3		
$LaCoO_3$	10.4	La_2CuO_4	5.8	Nd_2CuO_4	0
P a.s.	10.2	P a.s.	5.9	P a.s.	0.11
P O_2	10.4	P O_2	6.2	P O_2	0.31

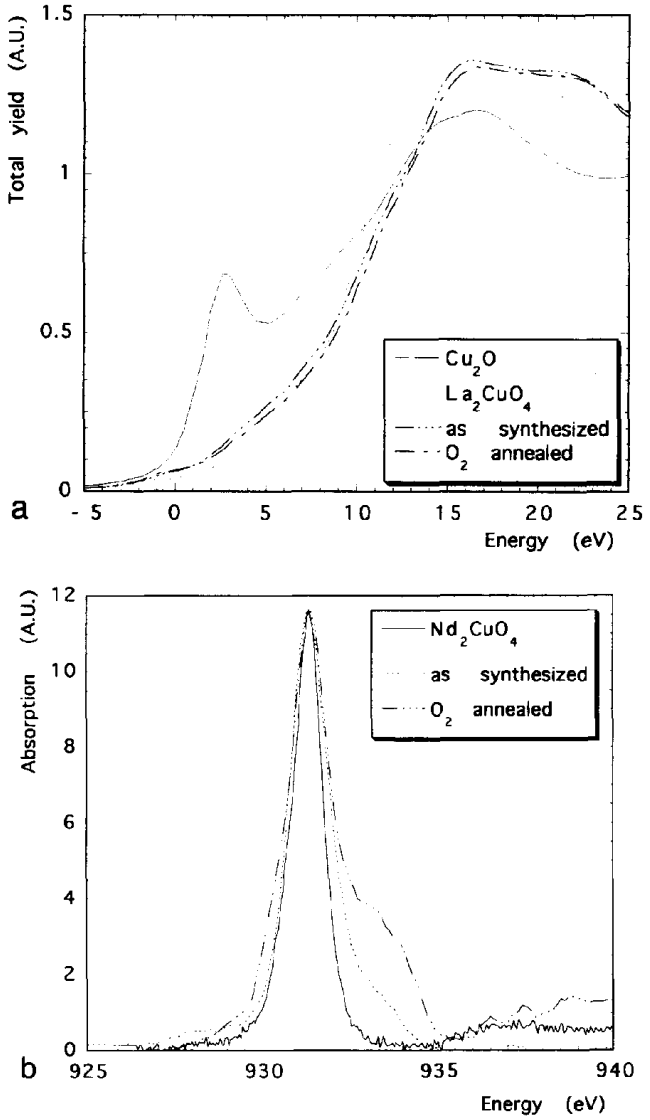

FIG. 6. (a) The CuK-edges of Cu_2O and La_2CuO_4, taken as references for Cu(I) and Cu(II) valence states, respectively, and of the $La_{0.2}Sr_{0.8}Cu_{0.4}Co_{0.6}O_{3-y}$ phase as synthesized and annealed at 450°C for 24 hr under 1 bar oxygen pressure. (b) The CuL_3-edges of Nd_2CuO_4, taken as reference for Cu(II), and of the $La_{0.2}Sr_{0.8}Cu_{0.4}Co_{0.6}O_{3-y}$ phase as synthesized and annealed under 1 bar oxygen pressure, showing the strong increase in the $|3d^9\underline{L}\rangle$ contribution in the latter case with respect to the as-synthesized compound.

for the as-synthesized $La_{0.2}Sr_{0.8}Cu_{0.4}Co_{0.6}O_{3-y}$ oxide and as a much stronger, large peak for the O_2-annealed one; a simulation with two Lorentzians gives 11% Cu(III) with respect to total copper for the former and 31% Cu(III) for the latter. These spectra confirm again that the oxidation of copper ions is due to a charge-transfer mechanism predominant in this oxygen-deficient cubic perovskite, such as that in HTC superconductors.

Moreover, the large linewidths of both lines, clearly visible in the spectrum of the O_2-annealed perovskite (Fig. 6b) with respect to Nd_2CuO_4, indicate a broad distribution of the oxygen surrounding the copper atoms.

The results of this XAS study of the $La_{0.2}Sr_{0.8}Cu_{0.4}Co_{0.6}O_{3-y}$ oxide can be summarized as follows:

(a) the cobalt atoms keep the mean Co(III) valence state, but with a reduced coordination number, five or four being possible.

(b) the estimated densities of doping holes per copper show that copper ions are oxidized before cobalt ions. Using the above results, one obtains oxygen stoichiometries of 2.42 and 2.46 for as-synthesized and O_2-annealed samples, respectively, this is in good agreement with the analytical values. In the O_2-annealed compound, the inserted oxygens are randomly distributed, with the Cu(III) species probably in octahedra and the Cu(II) still keeping the fivefold coordination.

3. Magnetic Susceptibility

The magnetic susceptibility was measured for both cobalt- and iron-substituted materials as synthesized. The thermal variations are plotted in Fig. 7. Both compounds exhibit a paramagnetic behavior above room temperature. At lower temperatures, the curves deviate from the Curie–Weiss law and on evaluation of the Weiss temperatures Θ_p (Table 3) shows that they are highly negative. This suggests antiferromagnetism ordering; such orderings were often observed for iron- and cobalt-based materials. The molar Curie constants (C_M) are reported in Table 3.

Assuming, as previously done (11, 12), that the copper contribution to the magnetic susceptibility is negligible,

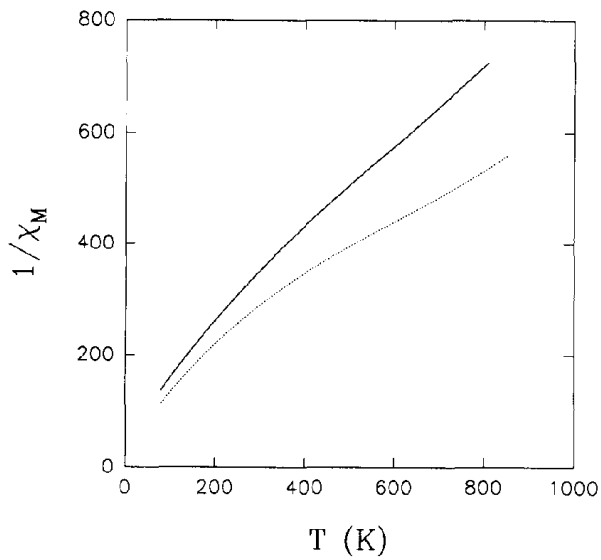

FIG. 7. χ_M^{-1} (mole · emu^{-1}) versus T (K) for as-synthesized samples. Dark lines and dotted lines correspond to $La_{0.2}Sr_{0.8}Cu_{0.4}Co_{0.6}O_{3-y}$ and $La_{0.2}Sr_{0.8}Cu_{0.4}Fe_{0.6}O_{3-y}$, respectively.

TABLE 3
Results of Magnetic Susceptibility Measurement: Experimental and Calculated Curie Constants for As-Synthesized $La_{0.2}Sr_{0.8}Cu_{0.4}M_{0.6}O_{3-y}$ Compounds (M = Fe, Co)

	C_M	C_{eqM}	Θ_p (K)
M = Co	1.1	1.83	−200
M = Fe	2.1	3.50	−370

owing to the existence of Cu(II)/Cu(III) mixed valency, the Curie constant per equivalent of cobalt and iron (C_{eqM}) can be calculated. The values are also reported in Table 3.

The experimental calculated Curie constant per cobalt (C = 1.83) is quite different from that expected for trivalent cobalt in high-spin (C = 3.0), intermediate-spin (C = 0.98), or low-spin configurations (C = 0). However, it is very close to that observed for the low-temperature form of $SrCoO_{2.5}$ (35, 36) (C = 1.62), in which cobalt is also trivalent. This value can be interpreted as a mixture of two different spin configurations for cobalt. A good agreement (C = 1.98) is obtained if we consider that 2/3 of cobalt exhibits high-spin configuration and 1/3 of cobalt exhibits low-spin configuration. These values correspond to 0.4 and 0.2 cobalt atoms per unit cell, respectively. Therefore, the presence of two spin configurations could be associated with the presence of copper in the perovskite framework and of oxygen vacancies which are probably in the vicinity of copper atoms.

In the case of iron-substituted oxide, Mössbauer spectroscopy, as will be shown below, and oxygen stoichiometry determination lead to about 60% Fe(IV) and 40% Fe(III). The resulting Curie constant per equivalent Fe, calculated assuming Fe(IV) and Fe(III) in high-spin configuration (C = 3.0 and C = 4.35, respectively), is C = 3.54; it is close to that deduced from magnetic susceptibility measurements (C = 3.50) (Table 3). High-spin Fe(III) and Fe(IV) have already been observed in other ferrocuprates with oxygen-deficient perovskite structures, such as $SrFe_{1-x}Cu_xO_{2.5-x/2+\delta}$ (11) and $Ba_{0.5}La_{0.5}Fe_{1-x}Cu_xO_{2.75-x/2+\delta}$ (12).

4. Mössbauer Spectroscopy

The Mössbauer spectrum of the $La_{0.2}Sr_{0.8}Cu_{0.4}Fe_{0.6}O_{2.64}$ phase recorded at room temperature is shown in Fig. 8a. It can be deconvoluted into three components with the same linewidth Γ. Their parameters are given in Table 4. The chemical isomer shifts δ, referred to metal iron, remain nearly constant ($\delta \approx 0.12$ mm/sec), but are much smaller than the classical value of the Fe^{3+}(S = 5/2) site ($\delta_{Fe^{3+}} \approx 0.3$ mm/sec). In any case, they are very close to those obtained for the average valence, $Fe^{3.5+}$, observed in the $SrFeO_{3-y}$ system (37). In the latter system, the average valence probably results from a fast hopping of an e_g electron between equal numbers of Fe^{3+} and Fe^{4+} ions in high spin state.

We can also suggest a significant delocalization and possible mixed valence state within the FeO_n polyhedra, assuming 50% Fe^{4+} + 50% Fe^{3+} in our compound. This ratio is slightly different from the analytical result (60% Fe^{4+} + 40% Fe^{3+}).

However, the quadrupole splitting values of the three iron sites are very different. The first component consists in a single line (ΔE = 0), which probably characterizes a regular octahedral environment whereas the two latter components with ΔE = 0.44 and 0.82 mm/sec can be identified as a more distorted octahedron and a pyramidal coordination of iron, respectively.

This point of view agrees with the Mössbauer results obtained for the compound annealed under oxygen pressure. The fitting of the corresponding spectrum (Fig. 8b) indicates the presence of the same sites, but the intensity of the second site slightly increases whereas the amount of the third one decreases. Moreover, their isomer shift and quadrupole splitting values are weaker than those observed for the sample synthesized in air (Table 4). This suggests that the FeO_n polyhedra are more regular in the oxygenated phase.

5. Electrical Measurements

The temperature dependence of the electrical conductivity shows in both cases a semiconducting behavior for the as-synthesized compounds whereas a tendency to semimetallic behavior is observed after oxygen annealing. At the same time, the room-temperature electrical conductivity increases (Table 5); however, σ values should only be considered as approximate values because of the difficulty in obtaining well-sintered ceramics, especially for the cobalt-substituted compound, as shown from the density measurements of the ceramics, which are in the ranges 80–85% and 70–75% for iron and cobalt samples, respectively.

TABLE 4
Mössbauer Parameters at Room Temperature of $La_{0.2}Sr_{0.8}Cu_{0.4}Fe_{0.6}O_{3-y}$ Compounds

Compounds	Site	$\delta \pm 0.01$ (mm/sec)	$\Gamma \pm 0.01$ (mm/sec)	$\Delta E \pm 0.01$ (mm/sec)	Fitted intensity ± 2(%)
Air	1	0.12	0.37	0.00	29
	2	0.13	0.37	0.44	38
	3	0.13	0.37	0.82	33
Oxygen	1	0.11	0.33	0.00	28
	2	0.11	0.33	0.35	42
	3	0.09	0.33	0.70	30

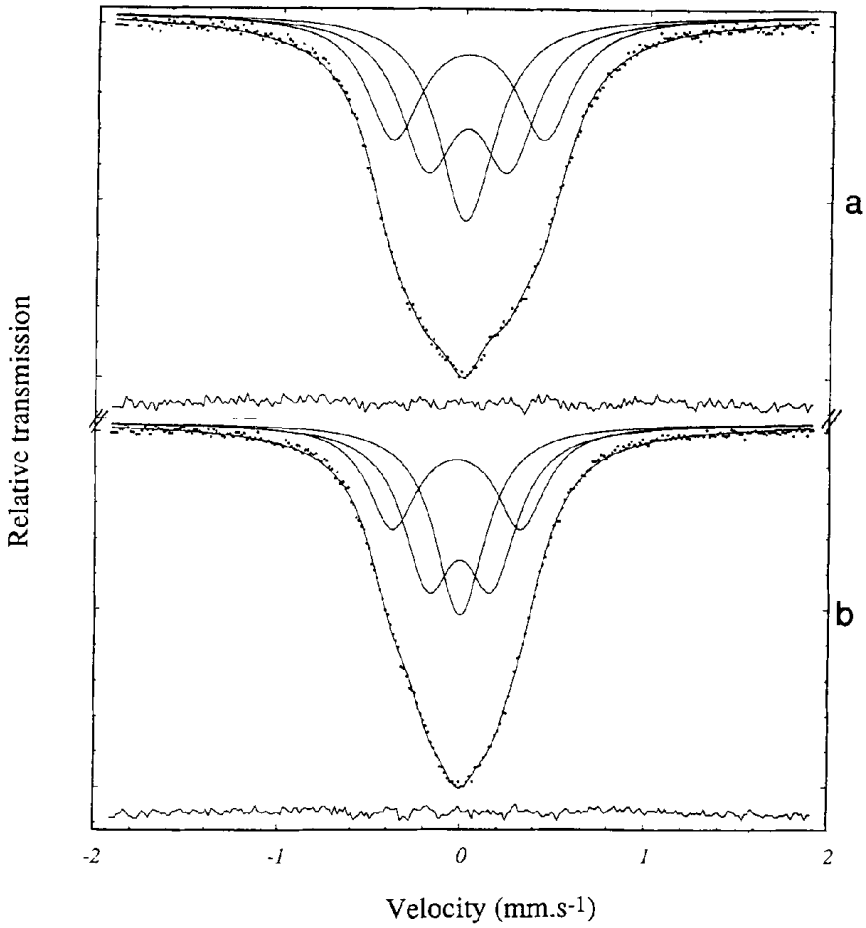

FIG. 8. Fitted Mössbauer data collected at room temperature for $La_{0.2}Sr_{0.8}Cu_{0.4}Fe_{0.6}O_{3-y}$:(a) as-synthesized sample, (b) O_2-annealed sample. Mössbauer parameters are given in Table 4.

The plots $\ln \sigma = f(1/T)$ (Figs. 9a and 9b) show that, whatever the thermal treatment is, an activation energy remains present in the conducting process. The curvature $\ln \sigma = f(1/T)$, which is obvious for the as-synthesized cobalt-substituted sample (Fig. 9a), suggests a variable range-hopping phenomenon at low temperature. Thus, the activation energy can only be calculated in the "high" temperature range, depending on the oxygen stoichiometry. The ΔE values are listed in Table 5.

Comparing the conductivity values at room temperature for the iron-substituted compound with those measured for the tetragonal phase $Sr_{1.6+x}La_{6.4-x}Cu_{8-x}Fe_xO_{20}$ ($x = 2.0$), the following comments can be made:

(i) The conductivity is lower for the as-synthesized cubic phase than for the tetragonal one, in spite of the presence of iron-mixed valency in the former and a larger number of oxygen vacancies in the latter. This difference is easily explained by the fact that the cubic perovskite exhibits a higher iron content and a statistical distribution of iron over the *B* sites, whereas iron only occupies one kind of site in the tetragonal phase (13), so that the three-dimensional Cu–O network is much less affected in the latter. This is also consistent with our previous results on mixed copper–iron oxides: $Sr_{1.6+x}La_{6.4-x}Cu_{8-x}Fe_xO_{20}$ (13), for which σ_{300K} decreases when the copper content decreases, and $Ba_{0.5}La_{0.5}Fe_{1-x}Cu_xO_{2.75-x/2+\delta}$ (12), where the conductivity was increased by a factor of 100 as soon as 10% of the iron was replaced by copper.

(ii) The conductivity is very sensitive to the annealing treatment. This phenomenon is easy to understand. In the case of the tetragonal phases, the oxygen stoichiometry remains close to 20 whereas it varies for the cubic phase, inducing a variation in the mean oxidation state of the transition cations. As shown from the Mössbauer spectroscopy study, iron is not drastically affected by the oxygen stoichiometry. Thus, an increase in the oxygen content involves an increase in the formal trivalent copper, leading to an increase in the conductivity and to a tendency to a metallic behavior.

$LaCoO_3$ (38) and $SrCoO_{2.5}$ (35), which are characterized

TABLE 5

Room Temperature Conductivity ($\Omega^{-1} \cdot cm^{-1}$) and Activation Energies (eV) ($T > 100$ K) for the Perovskites $La_{0.2}Sr_{0.8}Cu_{0.4}M_{0.6}O_{3-y}$ (M = Co, Fe)

	M = Co		M = Fe	
	σ	ΔE	σ	ΔE
a.s.[a]	2.4	0.097	7.6	0.036
O_2	8.4	0.004	64	0.014
10b	35	0.005	93	0.007
100b	137	0.009	85	0.004

[a] a.s. denotes the as-synthesized sample.

by trivalent cobalt, are poor conductors, $\sigma \approx 10^{-5}\Omega^{-1} \cdot cm^{-1}$ and $5 \times 10^{-2}\Omega^{-1} \cdot cm^{-1}$, respectively, at room temperature. So we can admit that the high conductivity measured for our as-synthesized and O_2-annealed oxides, also characterized by Co(III), is due to the presence of the mixed valence Cu(II)/Cu(III). This assumption can be extended to the 10b and 100b O_2-annealed compounds; however, for the latter a partial oxidation of Co(III) in Co(IV) must occur to satisfy the oxygen stoichiometry. Mixed valency Co(III)/Co(IV) oxides with a perovskite structure, such as $La_{1-x}Sr_xCoO_3$ (39) and $SrCoO_{3-x}$ (35), are metallic conductors. Consequently, the electrical behavior of 10b and 100b O_2-annealed compounds can then be interpreted as the consequence of the increase in the number of charge carriers due to the increase in Cu(III) and to the appearance of Co(IV), but also to a better delocalization of the charge carriers due to the decrease in the oxygen vacancies.

CONCLUDING REMARKS

We have prepared and studied two highly oxygen-deficient cubic perovskites in the systems La–Sr–Fe–Cu–O and La–Sr–Co–Cu–O. As prepared samples are both characterized by copper mixed valency, but they differ by the oxidation state of iron (mixture of Fe(III) and Fe(IV)) and of cobalt (only Co(III)). This confirms that iron is more easily oxidized than cobalt in these oxides, under normal conditions, with Co(IV) appearing only after being annealed under several bars oxygen pressure. The X-ray absorption spectroscopy study of two cobalt samples, as-synthesized and oxygen-annealed samples, shows that copper is more sensitive than cobalt to the oxygen pressure conditions. The same behavior is suggested by Mössbauer spectroscopy for the iron-substituted materials. Thus, the evolution of the transport properties with the annealing conditions is mainly due to the variation in the Cu(III)/Cu(II) ratio. This is in agreement with the results observed for other transition-metal-substituted cuprates.

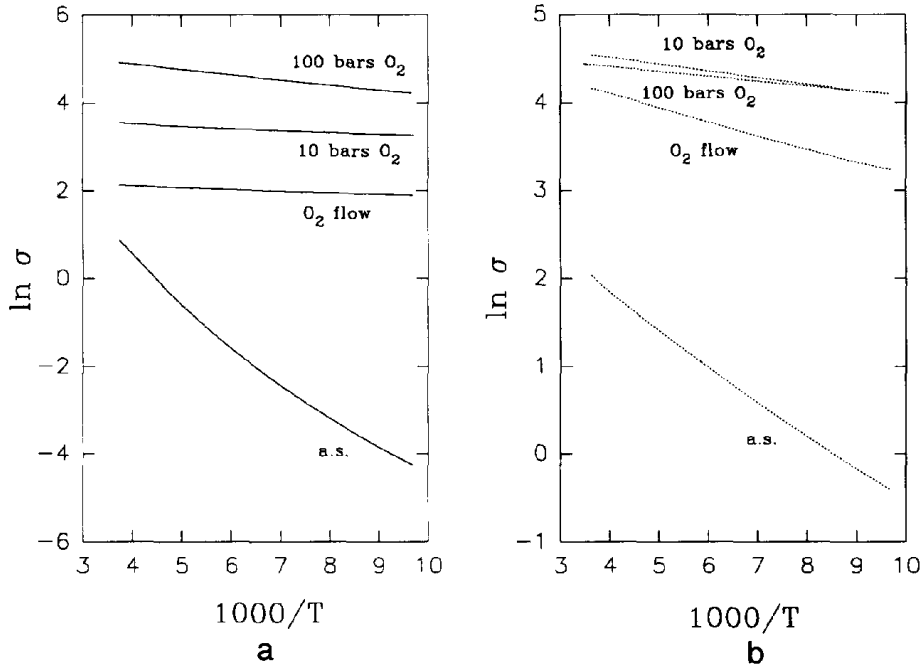

FIG. 9. Logarithm of the conductivity (in $\Omega^{-1} \cdot cm^{-1}$) versus $1000/T$ (K^{-1}) for as-synthesized samples and annealed samples under different oxygen pressures: (a) cobalt-substituted cuprates and (b) iron-substituted cuprates.

REFERENCES

1. J. B. MacChesney, R. C. Sherwood, and J. F. Potter, *J. Chem. Phys.* **43**(6), 1907 (1965).
2. B. C. Tofield, C. Greaves, and B. E. F. Fender, *Mater. Res. Bull.* **10,** 737 (1975).
3. C. Michel, L. Er-Rakho, and B. Raveau, *Mater. Res. Bull.* **20,** 667 (1985).
4. C. Michel, L. Er-Rakho, M. Hervieu, J. Pannetier, and B. Raveau, *J. Solid State Chem.* **68,** 143 (1987).
5. L. Er-Rakho, C. Michel, J. Provost, and B. Raveau, *J. Solid State Chem.* **37,** 151 (1981).
6. J. Provost, F. Studer, C. Michel, and B. Raveau, *Synth. Met.* **4,** 147 (1981).
7. B. Raveau, C. Michel, M. Hervieu, and D. Groult, "Crystal Chemistry of High Tc Superconducting Cuprates." Springer Series in Material Sciences, Vol. 15, Springer-Verlag, Berlin/New York, and references therein.
8. L. Er-Rakho, C. Michel, and B. Raveau, *J. Solid State Chem.* **73,** 514 (1988).
9. C. Michel, L. Er-Rakho, and B. Raveau, *J. Phys. Chem. Solids* **49**(4), 451 (1988).
10. J. B. Goodenough, *Prog. Solid State Chem.* **5,** 340 (1971).
11. L. Er-Rakho, C. Michel, F. Studer, and B. Raveau, *J. Phys. Chem. Solids* **49**(9), 1101 (1988).
12. L. Er-Rakho, C. Michel, F. Studer, and B. Raveau, *J. Phys. Chem. Solids* **48**(4), 377 (1987).
13. R. Genouel, C. Michel, N. Nguyen, M. Hervieu, and B. Raveau, *J. Solid State Chem.* **115,** 469 (1995).
14. D. B. Wiles and R. A. Young, *J. Appl. Crystallogr.* **540,** 259 (1981).
15. A. Bianconi, J. Budnick, A. M. Flank, A. Fontaine, P. Lagarde, A. Marcelli, H. Tolentino, B. Chamberland, G. Demazeau, C. Michel, and B. Raveau, *Phys. Lett. A* **127,** 285 (1988).
16. E. E. Alp, G. L. Goodman, L. Soderholm, H. B. Schuttler, S. M. Mini, M. Ramanathan, G. K. Shenoy, and A. S. Bommannavar, *J. Phys. Condens. Matter* **1,** 6463 (1989).
17. F. Baudelet, G. Collin, E. Dartyge, A. Fontaine, J. P. Kappler, G. Krill, J. P. Itie, J. Jegoudez, M. Maurer, Ph. Monod, A. Revcolevski, H. Tolentino, G. Tourillon, and M. Verdaguer, *Z. Phys. B* **69,** 141 (1988).
18. A. Bianconi, A. Clozza, A. Castellano, S. Dellalonga, M. De Santis, A. Dicicco, K. Garg, P. Delocv, A. Gargano, R. Giorgi, P. Lagarde, A. M. Flank, and A. Marcelli, *J. Phys. C* **9,** 1179 (1988).
19. T. Gourieux, G. Krill, M. Maurier, M. F. Ravet, A. Menny, H. Tolentino, and A. Fontaine, *Phys. Rev. B* **37,** 7516 (1988).
20. H. Tolentino, A. Fontaine, A. M. Flank, P. Lagarde, J. Y. Henry, J. Rossat-Mignod, T. Gourieux, G. Krill, and F. Studer, "IWEPS,90, Proceedings of the International School on Electronic Properties of High Tc Superconductors, Kirschberg, Austria" Springer Series of Solid State Sciences, Springer-Verlag, Berlin/New York, 1990.
21. B. Raveau, C. Michel, M. Hervieu, J. Provost, and F. Studer, "Earlier and Recent Aspects of Superconductivity" (J. G. Bednorz and K. A. Müller, Eds.), Springer Series in Solid State Sciences, Vol. 90, p. 66. Springer-Verlag, Berlin/New York, 1990.
22. R. Retoux, F. Studer, C. Michel, B. Raveau, A. Fontaine, and E. Dartyge, *Phys. Rev. B* **41,** 193 (1990).
23. J. van Elp, Ph.D. Thesis, "The Electronic Structure of Doped Late Transition Metal Monoxides," University of Groeningen, 1991.
24. V. Briois, C. Cartier, M. Momenteau, Ph. Maillard, J. Zarembovitch, E. Dartyge, A. Fontaine, G. Tourillon, P. Thiry, and M. Verdaguer, *J. Chim. Phys.* **86**(7/8), 1623 (1989).
25. L. Barbey, N. Nguyen, V. Caignaert, F. Studer, and B. Raveau, *J. Solid State Chem.* **112,** 148 (1994).
26. N. Menyuk, K. Dwight, and P. M. Raccah, *J. Phys. Chem. Solids* **28,** 549 (1967).
27. A. Bianconi, A. Congiu-Castellano, M. de Santis, P. Rudolf, P. Lagarde, A. M. Flank, and A. Marcelli, *Solid State Commun.* **63**(11), 1009 (1987).
28. A. Bianconi, A. Congiu-Castellano, M. de Santis, P. Delogu, A. Gargano, and R. Giorgi, *Solid State Commun.* **63**(12), 1135 (1987).
29. P. Kuiper, G. Kruizinga, J. Ghijsen, G. A. Sawatzky, and H. Verweij, *Phys. Rev. Lett.* **62**(2), 221 (1989).
30. A. Krol, C. S. Lin, Z. H. Ming, C. J. Sher, Y. H. Kao, C. T. Chen, F. Sette, Y. Ma, G. C. Smith, Y. Z. Zhu, and D. T. Shaw, *Phys. Rev. B* **42**(4), 2635 (1990).
31. A. Bianconi, M. De Santis, A. Di Dicco, A. M. Flank, A. Fontaine, P. Lagarde, H. Katayama-Yoshida, A. Kontani, and A. Marcelli, *Phys. Rev. B* **38**(10), 7196 (1988).
32. A. M. Flank, P. Lagarde, A. Bianconi, P. Castrucci, A. Fabrizi, M. Pompa, H. Katayama-Yoshida, and G. Calestani, *in* "Proceedings, 9th International Conference on Vacuum Ultraviolet Radiation Physics, Honolulu, July 17–21, 1989"; *Phys. Scr.* **41,** 901 (1990).
33. F. Studer, N. Merrien, C. Martin, C. Michel, and B. Raveau, *Physica C* **178,** 324 (1991).
34. N. Merrien, F. Studer, A. Maignan, C. Martin, C. Michel, B. Raveau, and A. M. Flank, *J. Solid State Chem.* **101,** 237 (1992).
35. T. Takeda and H. Watanabe, *J. Phys. Soc. Jpn.* **33**(4), 973 (1972).
36. J. C. Grenier, S. Ghodbane, G. Demazeau, M. Pouchard, and P. Hagenmüller, *Mater. Res. Bull.* **14,** 831 (1979).
37. L. Fournès, Y. Potin, J. C. Grenier, G. Demazeau, and M. Pouchard, *Solid State Commun.* **162**(4), 239 (1987).
38. P. M. Raccah and J. B. Goodenough, *J. Appl. Phys.* **32**(2), 1209 (1968).
39. J. B. Goodenough, *Prog. Solid State Chem.* **5,** 333 (1971).